Study of the influence of rheological parameters on the behavior of a submarine debris flow

Marcelo Muta Hotta[1#] (iD), Marcio de Souza Soares de Almeida[1] (iD),

José Renato Moreira da Silva de Oliveira[1] (iD), Ricardo Garske Borges[2] (iD)

Article

Abstract
Submarine debris flows are events that occur with great frequency on a geological scale and can cause major damage to offshore structures or even loss of human life. Understanding the mechanisms involved in the development of a debris flow requires not only knowledge of soil mechanics, but also knowledge of fluid mechanics, since the incorporation of water during the flow causes changes in shear strength. Unlike soils, the shear strength of fluids is represented by mathematical models called rheological models. The objective of this paper is to propose a new rheological model capable of representing the changes caused by water entrainment into a submarine debris flow, by correlating it with the Liquidity Index of the soil. A rheological analysis of marine clay samples from the pre-salt layer has made it possible to represent the variation in strength due to water content. The influence of water content and velocity on flow behavior has also been studied through the analysis of centrifuge tests performed in a previous study.

1. Introduction

Submarine debris flows consist of a mixture of sediment and water that is governed by gravity and is highly mobile due to voids filled with water and mud (Takahashi, 2007). These events pose a significant risk to offshore structures and can have catastrophic consequences for coastal communities (Locat & Lee, 2005; Tailling et al., 2012; Satake, 2012). However, their large size, usually associated with submarine geomorphology, and the great depths at which they occur, typically over 1000 m, make it difficult to monitor these events. As a result, most observations occur after a disaster and are only recorded as a result of damage or failure of seafloor structures such as internet cables and pipelines (Hsu et al., 2008).

Therefore, in order to mitigate environmental and financial damage, several research groups around the world have focused on understanding the development of these phenomena and their consequences. Heezen & Ewing (1952) studied the 1929 Grand Banks debris flow in Canada, caused by a magnitude 7.2 earthquake, where some telephone cables were broken. Another similar case occurred in 2006 off the coast of Taiwan (Hsu et al., 2008), where several debris flows severed internet cables, only to be assessed after the disaster. Locat & Lee (2002) report that

in 1929 an earthquake generated a debris flow that destroyed submarine communication cables about 1000 km from the epicenter. Another more recent case occurred in 1998, when a submarine landslide triggered by an earthquake caused a tsunami that killed about 2,500 people in Papua New Guinea (Heidarzadeh & Satake, 2015).

Guo et al. (2020) pointed out the need to improve the understanding of the stages of a submarine debris flow as well as the forces acting throughout the flow. There is also a need for a better calculation of the effects of water entrainment on the shear strength of the material. To this end, it is important to consider the soil from a fluid mechanics perspective (Tsugawa et al., 2019).

In this context, rheology is a significant tool for understanding the factors that govern debris flows, such as the incorporation of water and the identification of turbidity currents. It provides parameters for physical and numerical modeling (Zakeri et al., 2010; Liu et al., 2020). However, studies have shown that rheological models used to describe fluids with yield stress do not have a good correlation between rheological and geotechnical properties. Therefore, several studies have aimed to develop more suitable rheological models (Imram et al., 2001; De Blasio et al., 2003; Jeong, 2014; Campos & Galindo, 2016). The present study involves a rheological analysis of marine clay samples collected from

#Corresponding author. E-mail address: hottamar@gmail.com
[1]Universidade Federal do Rio de Janeiro, Programa de Pós-graduação em Engenharia Civil, Rio de Janeiro, RJ, Brasil.
[2]Petrobras, Centro de Pesquisa e Desenvolvimento, Rio de Janeiro, RJ, Brasil.

Hotta et al., Soil. Rocks, São Paulo, 2024 47(4):e2024001524

1

different points in the Campos Basin, with water depths greater than 1000 m and where a variety of offshore pre-salt oil exploration structures are located. The objective is to propose a new rheological model capable of representing the changes caused by water entrainment into a submarine debris flow (Widjaja & Lee, 2013), by correlating it with the Liquidity Index of the soil. This parameter is especially suitable for debris flow behavior studies, since it gives a measure of how far the water content is from the liquidity limit, therefore providing a direct quantification of the capability of the flow to behave as a fluid.

The use of the proposed model in the analysis of submarine debris flows will allow a more accurate simulation of the distance traveled by the flow and the risks associated with the submarine slope failure for offshore structures, since the existing models do not take into account the water entrainment into the flow which is essential to predict its behavior.

2. Submarine debris flows

Early studies on submarine debris flows conducted by this research group using a beam centrifuge were reported by Acosta et al. (2017). Subsequently, Hotta et al. (2020) analyzed the process of transformation of debris flows into turbidity currents using a mini drum geotechnical centrifuge. This equipment has been applied in the last two decades to model a wide range of offshore problems (e.g. Oliveira & Almeida, 2010; Almeida et al., 2013; Rammah et al., 2014; Oliveira et al., 2017), but also onshore problems (e.g., Almeida et al., 2011; Fagundes et al, 2012).

2.1 The Anatomy of a submarine debris flow

The development of a submarine debris flow can be divided into 4 stages as shown in Figure 1. Stage 1, named Failure, (Figure 1a), begins with the triggering mechanism, which can be an earthquake, erosive processes, volcanism, human activities, among others (Locat & Lee, 2009), and ends with the onset of material displacement. This phase is governed by the laws of soil mechanics.

Stage 2 consists of the formation of the flow (Figure 1b) and begins with the sliding of the soil mass down the slope, which mixes with the water in the medium. This stage is also characterized by a reduction in the shear strength of the soil caused by the increase in water content, which exhibits transitional behavior from that of a solid to that of a non-Newtonian fluid.

Stage 3 is the longest and is associated with the development of the debris flow (Hotta et al., 2020). After this stage, the flow may continue as a submarine debris flow (Figure 1e), or it may become a turbidity current (Figure 1c) with a predominance of suspended particles, depending on the relationship between gravitational and viscous forces, represented by the Reynolds number.

In stage 4, deposition of the material occurs, the rheological properties of which were studied by Liu et al. (2020), who concluded that in less dense flows (turbidity currents) there is an accelerated dissipation of kinetic energy, i.e. deposition of soil occurs during the flow (Figure 1d). In submarine debris flows, which are denser in composition, deposition occurs at the stop of the flow due to friction of the basal layer of the flow with the seabed, resulting in the formation of large deposits (Dowdeswell et al., 1996; King et al., 1996; Vorren et al., 1988) and the transport of large volumes of soil (Figure 1f).

2.2 Rheological models in submarine flows

As in slope stability analysis, the shear strength of the fluid (soil and water) acts to resist movement. However, the water entrainment during flow causes constant changes in the composition and properties of the material (Liujun et al., 2023) (Figure 2), including a reduction in shear strength (Locat & Lee, 2009).
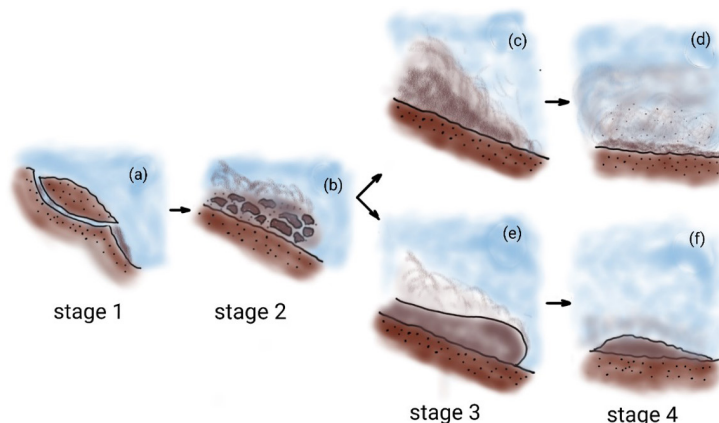

Figure 1. Stages of a submarine debris flow: (a) failure; (b) flow formation; (c) turbidity current; (d) deposition of suspended particles; (e) submarine debris flow; (f) formation of debris deposits.
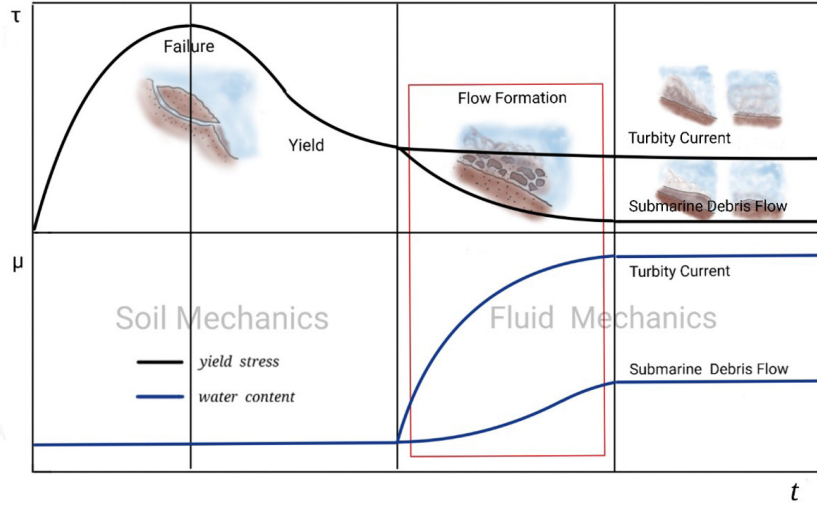
Figure 2. Shear strength behavior and variation in water content of the material during the development of a submarine debris flow.

Debris flows behave like a non-Newtonian fluid (Jeong et al., 2010), and like a fluid, their shear strength can be represented by rheological models. The Bingham model (Equation 01) is a widely used model due to its simplicity (Barnes, 1999). This model (Figure 3) has two rheological parameters: viscosity (μ) and yield stress (τ_0). The yield stress is the minimum shear stress required to initiate flow (Tsugawa et al., 2019). When the fluid is subjected to lower stresses, it behaves like a rigid elastic solid. Viscosity is the portion of the resistance that varies as a function of shear rate.

$$\tau = \tau_0 + \mu\dot{\gamma} \tag{1}$$

Another widely used model for debris flows is the bilinear model (Jeong, 2014), in which the fluid has two flow regimes: one for shear rates lower than the critical shear rate $\left(\dot{\gamma} < \dot{\gamma}_c\right)$, in which the material behaves like a Newtonian fluid (Regime I, Equation 02), and another for shear rates higher than the critical value (Regime II, Equation 03), in which the material behaves like a Bingham fluid (Salmanidou et al., 2018). Figure 3 shows the plot of the Bingham and bilinear models with Regimes I and II for the same flow curve. Thus, for $\left(\dot{\gamma} < \dot{\gamma}_c\right)$:

$$\tau = \mu_1\dot{\gamma} \tag{2}$$

and for $\left(\dot{\gamma} \geq \dot{\gamma}_c\right)$:

$$\tau = \tau_0 + \mu_2\dot{\gamma} \tag{3}$$

where: τ_c is the critical stress and represents the shear strength corresponding to the critical shear rate.

Debris flows are governed by the rheological parameters of the material, but other factors such as velocity, specific gravity of the soil, and channel geometry also affect the flow behavior.
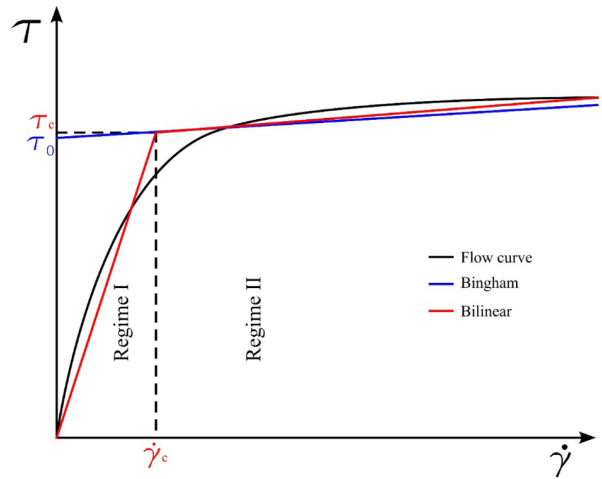

Figure 3. Flow Curve Example, Bingham Model, Bilinear Model - Regime I and II.

A dimensionless number that expresses the effect of varying each of these parameters is the Bingham Reynolds number ($R_{eBingham}$), calculated from Equation 04 (Madlener et al., 2009; Haldenwang & Slatter, 2006). A flow with a $R_{eBingham}$ greater than 1500 characterizes a semi-turbulent regime and indicates the formation of a turbidity current (Hotta et al., 2020), which causes an increase in water entrainment into the flow.

$$R_{eBingham} = \frac{\rho_s D_e v_m}{\mu + \dfrac{\tau_0(w)}{\dot{\gamma}(w)}} \tag{4}$$

where: ρ_s is the density of the slurry; v_m is the frontal velocity of the flow; μ is the dynamic viscosity; τ_0 is the yield stress; $\dot{\gamma}$ is the shear strain rate; and D_e is the equivalent diameter,

which is the ratio between the channel wet cross-section area and wet perimeter.

D_e is a relevant parameter in the calculation of the Reynolds number because, in an open channel, it indicates that reducing the flow height cause the increase in R_e, which may lead to a change in the flow behaviour from laminar to turbulent.

3. Rheological tests

This section describes the tests correlating the rheological parameters of marine clay samples from the Brazilian continental shelf with their respective liquidity indexes. Based on the results, a bilinear rheological model is proposed to account for water entrainment in debris flows.

3.1 Materials and methods

The rheological study of fine marine sediments is a topic addressed by several authors (Jeong et al., 2009, 2010; Zakeri et al., 2010). In this study, 6 soil samples from the Santos Basin, on the Brazilian continental shelf, were used for this purpose. The Santos Basin is the largest sedimentary offshore basin in Brazil and is one of its most important oil and gas exploration regions where the deepest platforms are installed.

The samples were taken in the seabed at depths of up to 30 m in regions with water depths of more than 1000 m and have the following average particle size distributions: 60% silt, 38% clay, and 2% sand. Analysis by electron microscopy and X-ray diffraction showed that the soil is composed mainly of SiO_2 and $CaCO_3$. Table 1 summarizes the geotechnical properties of these samples, which are classified as high plasticity inorganic clays according to the unified soil classification system (USCS) (ASTM D2487-2017), with the soil's Liquidity Index (*LI*) calculated using Equation 05.

$$LI = \frac{w - w_P}{w_L - w_P} \qquad (5)$$

where: w is the water content; w_P is the plastic limit; and w_L is the liquid limit.

Six reconstituted samples were prepared by remoulding the Shelby samples in a mixer for 30 minutes by adding destiled water. Then each of the 6 samples was tested with 3 different water contents, for a total of 18 tests.

A Brookfield RST-CC rheometer was used to perform the ramp and vane tests at a controlled laboratory temperature of 24°C. The well-known equations to compute shear stresses and shear strains for concentric cylinder (CC) and vane geometries are given by Steffe (1996). The ramp tests used a smooth concentric cylinder geometry (Figure 4a) consisting of an inner rotor and an outer cup of varying dimensions selected based on the magnitude of the apparent yield stress (τ_0) of the sample being tested, as each geometry is suitable for different stress ranges. The tests consisted of continuously and linearly increasing and decreasing the shear rate from 0 s^{-1} to 100 s^{-1} (acceleration) and from 100 s^{-1} to 0 s^{-1} (deacceleration) and measuring the corresponding shear stresses. The shear rate variation was 1s^{-1}/s. This range of shear rate values was defined based on recommendations in the literature for submarine debris flow events (Kobayashi et al., 2015; Santoro et al., 2012). The vane tests (Barnes & Nguyen, 2001; Steffe, 1996) were carried out at a constant shear rate of 0.1 s^{-1} and a constant temperature of 24°C to measure the shear strength τ_p of the samples. The vane geometries are shown in Figure 4b. The geometry chosen for the ramp and vane tests depends on the range of shear stresses being studied. In this case, given the specimens studied and the assumed fluidity index values, the CCT-25 and VT 30-15 geometries were used for the ramp and vane tests, respectively.

During ramp tests, flow curves are obtained that describe the behavior of soil as the shear rate varies from zero to the established limit and back to zero, i.e., when the soil is accelerating and decelerating, respectively. The authors aim to fill a gap in the existing literature by providing a detailed understanding of the curves that best represent each stage of the debris flow. Figure 5 shows the flow curves obtained in the ramp tests for soil samples 1, 2, 3, and 5, that correspond to the deceleration stretch and represent the behavior of the material during most of the flow.

Table 1. Geotechnical properties of the soil samples and adopted water content.

Sample	G_S	w_P (%)	w_L (%)	w_1 (%)	w_2 (%)	w_3 (%)
S1	2.69	39.0	117.0	107.1	124.3	140.5
S2	2.68	36.0	90.0	98.2	112.1	128.4
S3	2.70	30.0	82.0	97.0	112.4	132.2
S4	2.67	28.0	114.0	95.0	122.0	135.0
S5	2.72	23.0	67.0	99.7	117.8	133.1
S6	2.72	27.0	104.0	104.0	130.1	141.3

G_S = Specific gravity of soil; w_P = Plastic limit; w_L = Liquid limit.
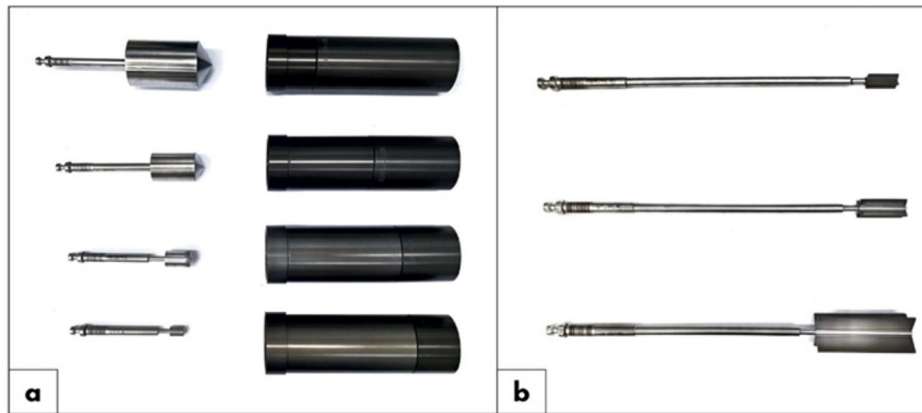
Figure 4. Geometries used in the tests (a) concentric cylinders (from top to bottom) CCT-40, CCT-25, CCT-14, CCT-8; (b) vane (from top to bottom) VT 20-10, VT 30-15, VT 60-30.
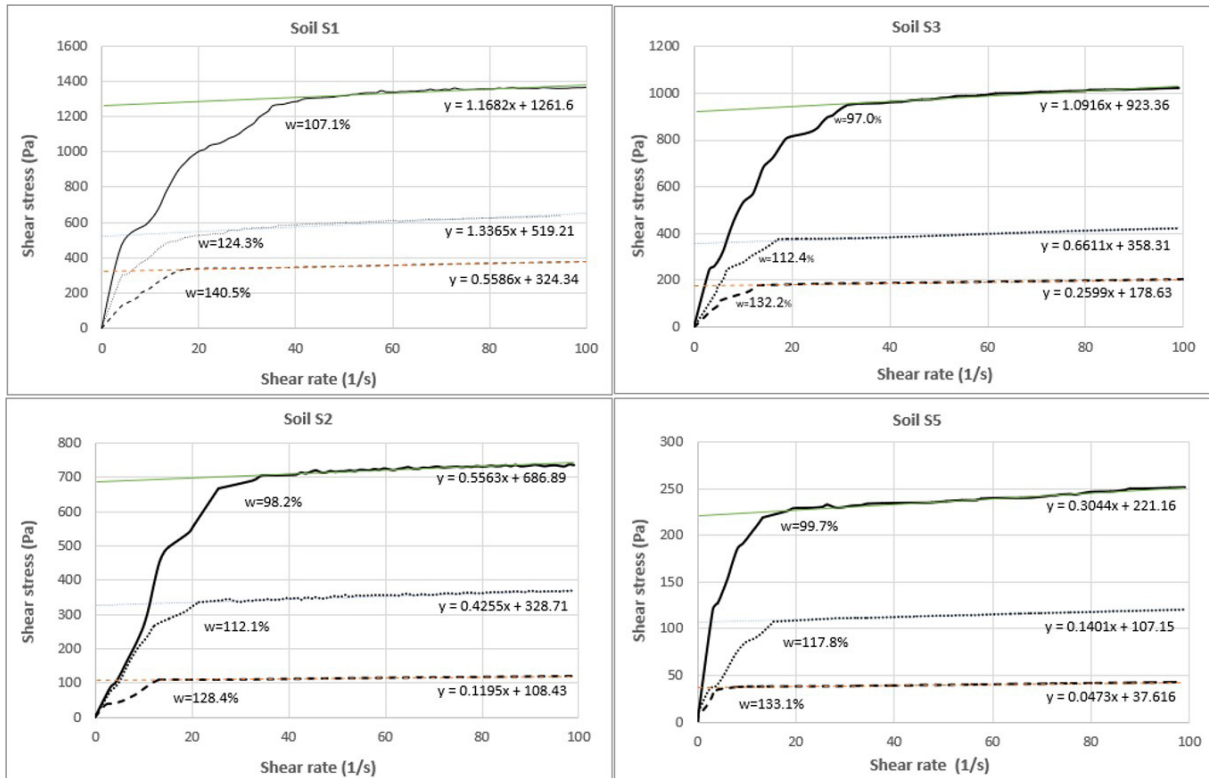

Figure 5. Flow curves for soil samples S1, S2, S3 and S5 and corresponding Bingham model lines.

3.2 Results of the rheological tests

The values of Bingham yield stress (τ_0), viscosity (μ) and critical flow rate ($\dot{\gamma}_c$) obtained in the ramp tests for each of the samples tested are shown in Table 2. As can be seen from the flow curves shown in Figure 5, the straight line assumed for regime II of the bilinear model and the straight line of the Bingham model are practically identical.

Therefore, to simplify the modeling, $\mu_2 = \mu$ and $\tau_0 = \tau_c$ are assumed (Table 2).

Figure 6 compares the remolded shear strength values (τ_p) from the vane tests with the yield stress measurements (τ_0) from the concentric cylinders (CC) tests. The average values differ by less than 15%. However, in tests with the lower water content (T1, T4, T7, T10, and T16), the concentric cylinder tests showed higher shear stresses due

Table 2. Parameters of the rheological model.

Samples		w (%)	τ_0 (Pa)	μ (Pa. s^{-1})	$\dot{\gamma}_c$ (s^{-1})	Samples		w (%)	τ_0 (Pa)	μ (Pa. s^{-1})	$\dot{\gamma}_c$ (s^{-1})
S1	T_1	107.1	1261.6	1.168	40.0	S4	T_{10}	95.0	1486.2	0.302	34.0
	T_2	124.3	519.2	1.337	25.0		T_{11}	122.0	503.3	0.589	24.0
	T_3	140.5	324.3	0.559	20.0		T_{12}	135.0	226.1	0.322	16.0
S2	T_4	98.2	686.9	0.556	32.0	S5	T_{13}	99.7	221.2	0.304	18.0
	T_5	112.1	328.7	0.426	24.0		T_{14}	117.8	107.2	0.140	15.0
	T_6	128.4	108.4	0.120	12.0		T_{15}	133.1	37.6	0.047	8.0
S3	T_7	97.0	923.4	1.092	24.0	S6	T_{16}	104.0	1092.4	0.509	25.0
	T_8	112.4	358.3	0.661	17.0		T_{17}	130.1	339.2	0.493	20.0
	T_9	132.2	178.6	0.260	14.0		T_{18}	141.3	163.8	0.260	13.0
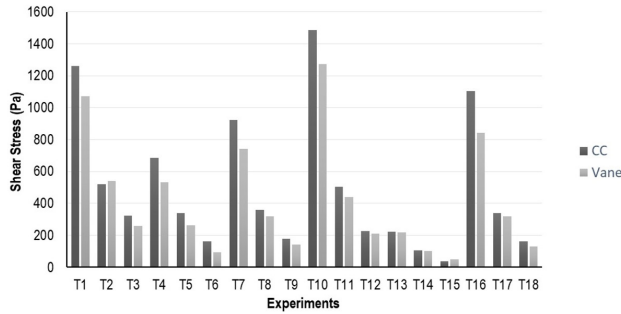
Figure 6. Comparison between the apparent yield stress (sweep tests) and remolded shear strength (vane tests) values for soil samples – "Bingham model".

to greater viscous effects (Sigh & Mitchell, 1968; Bjerrum, 1972; Chandler, 1988; Bowles et al., 2003; Yang et al., 2015).

The values of the rheological parameters τ_0, μ and $\dot{\gamma}_C$ (Table 2) and the correlation curves of these parameters with the liquidity index of the material are given in Equations 06, 07 and 08.

$$\tau_0 = 780.8\,LI^{-2.77} \tag{6}$$

$$\mu = 0.82\,LI^{-2.35} \tag{7}$$

$$\dot{\gamma}_C = 27.64\,LI^{-1.11} \tag{8}$$

As can be seen in Figure 7, the three rheological parameters decrease exponentially with the Liquidity Index of the material. Considering that, for a given soil, all the parameters of the bilinear model can be calculated as a function of the LI (Equations 06, 07 and 08), the rheological parameters can be correlated with the water content of the sample.
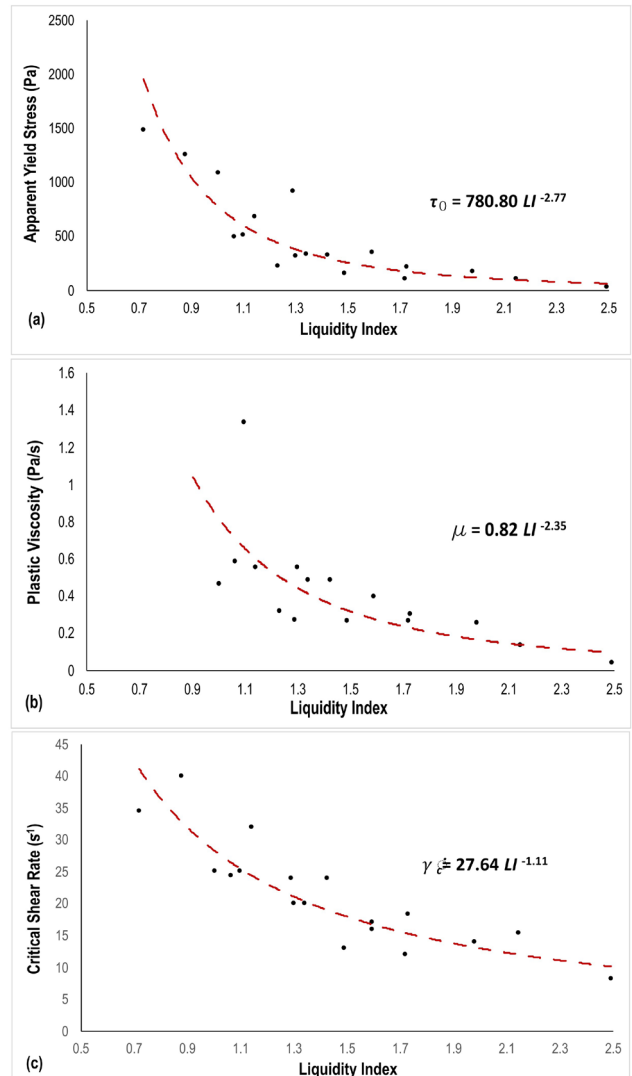
Figure 7. Rheological parameters versus liquidity index (a) apparent yield stress; (b) plastic viscosity; and (c) critical shear rate.

The correlation between the yield stress τ_0 and the *LI* (Figure 7a) given by Equation 6 is similar to that found for other soils (Locat, 1997; De Blasio et al., 2003; Issler et al., 2005; Sørlie et al., 2022). Other rheological studies (Campos & Galindo, 2016; Jeong et al., 2010; Jeong, 2014; Sørlie et al., 2022) have shown a similar relationship between the viscosity and the Liquidity Index (Figure 7b), for the range of *LI* values greater than 1.

3.3 Proposed bilinear model considering the soil Liquidity Index

Based on the tests presented, the influence of the water content of the material on the shear strength of the soil can be expressed by adopting a bilinear model in which the rheological parameters vary as a function of the water content of the material. For marine clays from the Santos Basin, the model is defined by equations 09, 10 and 11.

In regime II ($\dot{\gamma} > \dot{\gamma}_C$), substituting (06) and (07) in (03), we have:

$$\tau = 780.8\, LI^{-2.77} + 0.82\, LI^{-2.35}\dot{\gamma} \qquad (9)$$

τ_C can be calculated by substituting (08) into $\dot{\gamma}$ from (09):

$$\tau_c = 780.8\, LI^{-2.77} + 22.61\, LI^{-3.45} \qquad (10)$$

Finally, the shear strength τ corresponding to Regime I ($\dot{\gamma} < \dot{\gamma}_C$) can be calculated by:

$$\tau = 0.82\, LI^{-2.35}\dot{\gamma} \qquad (11)$$

The parametric analysis of equation 08 shows that the higher the water content of the mixture, the lower the transition shear rate ($\dot{\gamma}_C$) between regimes I and II, decreasing until the behavior of the material approaches the Bingham model (Figure 3). Therefore, the use of the bilinear model is recommended for the analysis of flows with low average velocity, i.e. with an average shear rate below the critical shear rate. In other cases, it is possible to use the Bingham model (Guo et al., 2020), which has the advantage of mathematical simplification since it contains only one regime.

The results show a good agreement between the model curves and the flow curves obtained in the tests, especially for the samples with the highest water content, which characterize a submarine debris flow. Figure 8 shows the comparison of a representative group of the flow curves obtained in the rheological tests (T2, T14 and T17) with those obtained using the adapted bilinear model, assuming different water contents.

The equations used to predict the flow curves in Figure 8 are valid only for the tested soil which parameters were obtained in the rheological tests. For different soils, new rheological tests are needed, and a new set of equations will be defined.

4. Assessment of the relevance of the model base on previous results

Given the difficulty in evaluating the geotechnical and rheological parameters of a real submarine flow, as mentioned above, centrifuge physical modeling was used to evaluate the relevance of the assumptions considered here. To that end, the tests carried out by Hotta et al. (2020) to study the dynamics of submarine flows were used to investigate the conditions for the formation of a turbidity current evaluating the relevance of water content to the behavior of this phenomenon, based on $R_{eBingham}$. Centrifuge tests were conducted using Speswhite kaolin clay, a commonly used soil in centrifuge modeling.
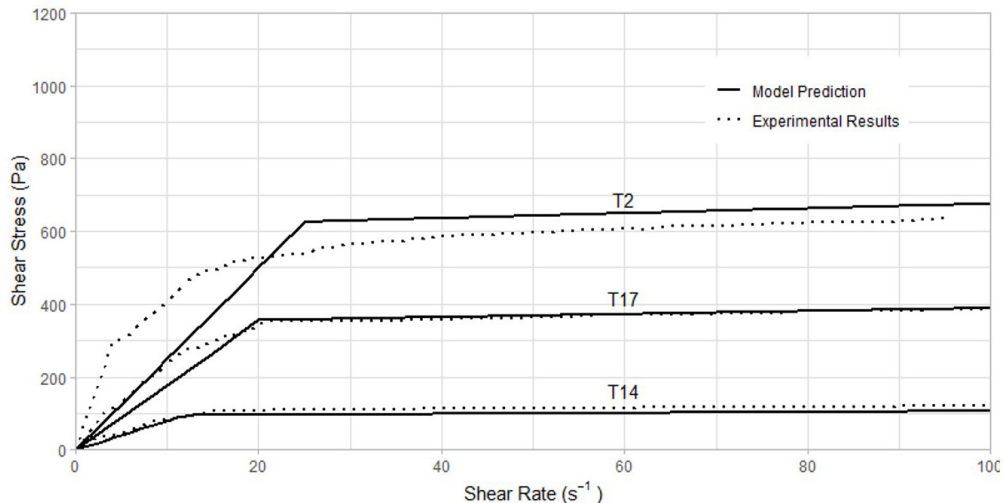

Figure 8. Comparison between model predictions and experimental results.

Table 3 shows the rheological parameters of the Speswhite clay for each water content value in the three tests performed by Hotta et al. (2020), obtained using the rheometer equipment and procedures described above.

Figure 9 depicts the test scheme analyzed according to the approach proposed in this article, and Table 3 shows the parameters of each test. The initial flow velocity, measured at checkpoint 1 (P_1 in Figure 9), was controlled by applying different mud launch pressures, and the rheological parameters were modified with the variation of the water content.
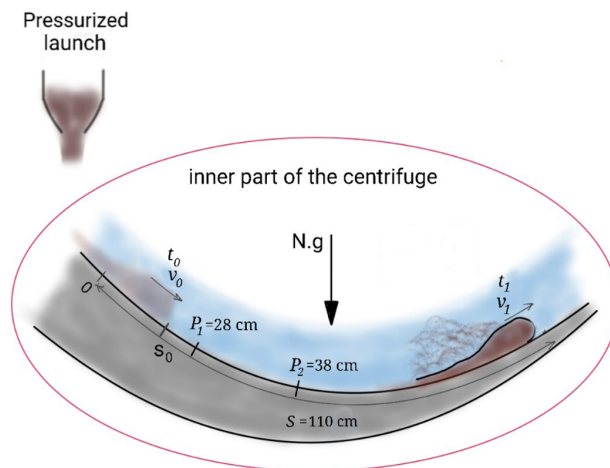

Figure 9. Representation of the kinematic parameters of a submarine debris flow in a centrifuge test. Based on Hotta et al. (2020).

Average velocity (v_m), yield stress (τ_0), viscosity (μ) and Bingham Reynolds number for each sample (Hotta et al., 2020) are listed in Table 3. It is important to note that both the viscosity and the yield stress are a function of the *LI* of the material.

As already explained, the most appropriate model to study the flows in stage I (Figure 1) would be the bilinear model. However, since the tests represent a high initial velocity flow, the use of the Bingham model satisfies the initial conditions of the problem, since flows with high initial velocity characteristics correspond to stages 3 and 4, where the shear rate is greater than the critical shear rate.

The comparison of tests w90_p0.8 and w100_p0.8 (Figures 10 and 11) shows the influence of the variation of the water content on the flow behavior since both were launched at the same pressure (same initial velocity) and with different water contents (Table 3). The flow velocities measured at checkpoint 1 (Table 3) were 0.39 m/s in test w90_p0.8 and 1.00 m/s in test w100_p0.8. In real scale, these two tests are equivalent to two flows formed by the same material, with the same initial velocity, developed on slopes with the same inclination (same inertial component), but with different water contents. This condition can be caused, for example, by the difference between the triggering mechanisms.

In test w90_p0.8, the flow developed as a submarine debris flow, represented by stage 3b in Figure 1. However, in test w100_p0.8, as a result of the increase in initial water content, the flow regime became turbulent and developed into a turbidity current, represented by stage 3a in Figure 1.
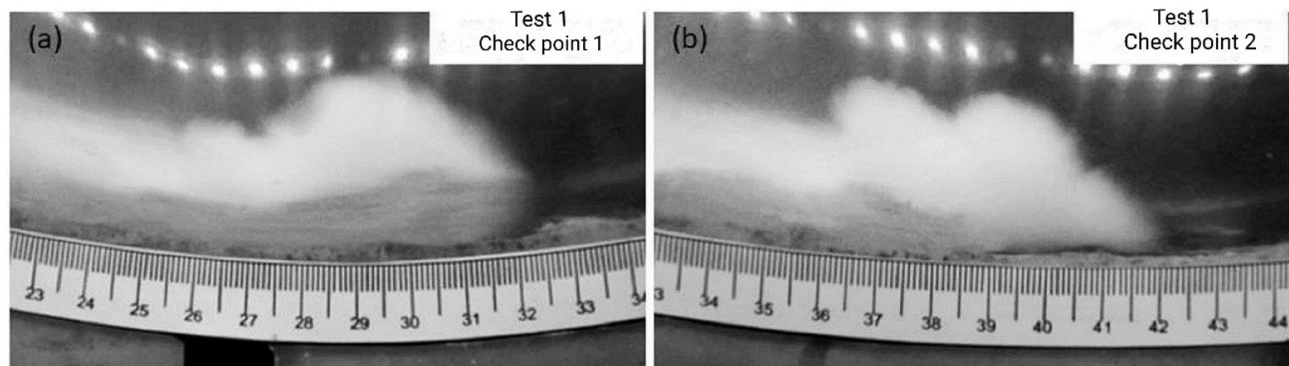

Figure 10. Image of test w90_p0.8 (w = 90%). (a) checkpoints 1; (b) check point 2. Adapted from Hotta et al. (2020).

Table 3. Centrifuge test parameters (Hotta et al., 2020).

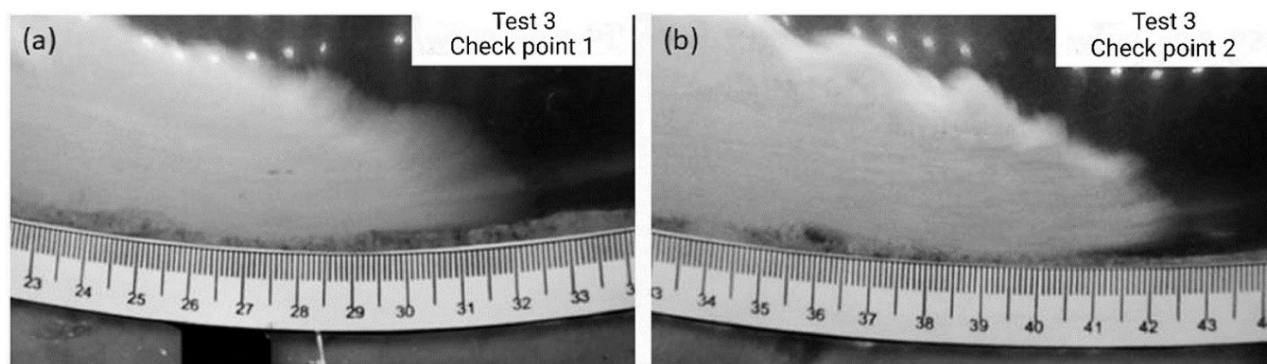| Test identification	Water content w (%)	Slurry yield stress τ_0 (Pa)	Slurry dynamic viscosity μ (Pa.s)	Applied pressure (kPa)	Velocity (m/s)	Bingham Reynolds Number
w90_p0.8	90	231	5.89	80	0.39	212.7
w90_p0.9	90	231	5.89	90	0.42	282.4
w100_p0.8	100	200	4.57	80	1.00	1816.2

Figure 11. Image of test w100_p0.8 (w = 100%). (a) check point 1; (b) check point (2). Adapted from Hotta et al. (2020).
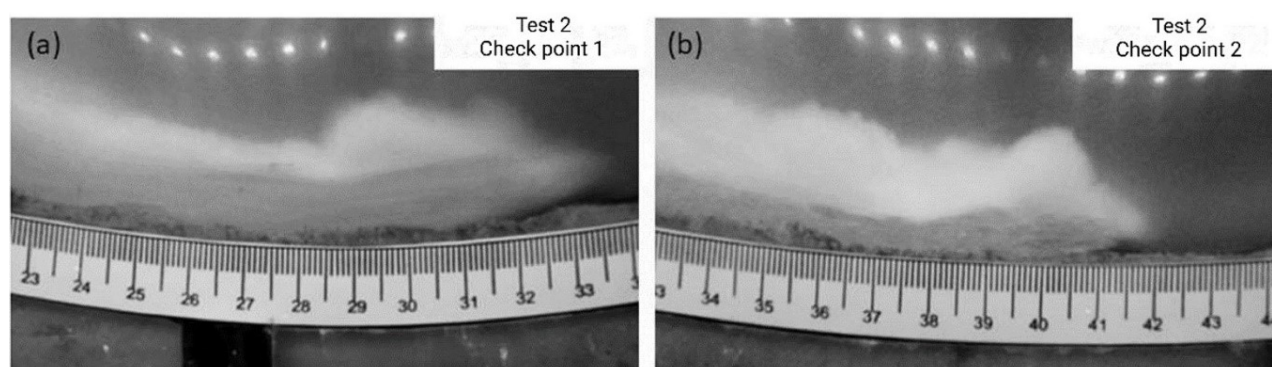

Figure 12. Image of test w90_p0.9 (w = 90%). (a) check point 1; (b) check point 2. Adapted from Hotta et al. (2020).

These results are consistent with the predictions based on the Bingham Reynolds number analysis ($Re_{Bingham} > 1500$).

By comparing tests w90_p0.8 and w90_p0.9 in Figure 10 and Figure 12, it is possible to see the isolated effect of the initial velocity of the flows, since they differ only in the launch pressure (initial velocity), the former being 80 kPa and the latter 90 kPa. The flow velocities measured at checkpoint 1 were close, despite the different launch pressures: 0.39 m/s for test w90_p0.8 and 0.42 m/s for test w90_p0.9. At real scale, these tests are equivalent to two flows of the same material with the same water content, differing only by different initial velocities. The comparison between Figures 11 and 12 shows that in neither test did the debris flow become a turbidity current, again confirming the predictions of a change in flow regime based on the Bingham Reynolds number.

The centrifuge tests confirm that, due to the exponential relationship between *LI* and shear strength, an 11% change in the water content of the material caused a change in the flow regime, which did not occur with the 12.5% increase in launch pressure from test w90_p0.8 to test w90_p0.9.

The results can be better understood by analyzing the influence of the variation of the velocity and the water content separately in the $Re_{eBingham}$. Equation 4 shows that $Re_{eBingham}$ increases linearly with velocity. In contrast, as

has been shown for the marine clay from the Brazilian pre-salt (Equations 10 and 11) and other soils studied in similar investigations, $Re_{eBingham}$ increases exponentially with increasing water content.

The transformation of the submarine debris flows into a turbidity current (Figure 1) causes an accelerated dissipation of kinetic energy, which translates into greater deceleration and lower run out. This confirms the need to use adaptive rheological models, such as the one presented, for the modeling, study and analysis of the risks caused by submarine debris flows in offshore installations.

5. Conclusions

The main conclusions of this research are:
- The proposed rheological model makes it possible to model the different stages of a debris flow, since both yield stress and viscosity (Bingham and Bilinear models) are replaced by a function correlated solely with the *LI* of the material. As such, it integrates the changes in rheological properties resulting from the incorporation of water into the medium.
- The bilinear model should preferably be used when modeling submarine debris flows in their initial phase,

Hotta et al., Soil. Rocks, São Paulo, 2024 47(4):e2024001524

9

since after the slope failure the velocity developed by the flow is not yet high, resulting in lower shear rates. In other cases, the model can be simplified to Bingham, which has the advantage of mathematical simplicity.

- The behavior of a submarine debris flow is very sensitive to changes in the water content of the material, since the Reynolds number increases linearly with increasing flow velocity but increases exponentially with increasing water entrainment.

- The use of the proposed model applied to the centrifuge tests conducted by Hotta et al. (2020) to calculate the Bingham Reynolds number allowed to interpret the changes in flow regime and better understand the behavior of the debris flow. The application of these concepts in numerical modeling and analysis of the risks caused by submarine debris flows provides greater security for offshore installations.

Acknowledgements

Declaration of interest

The authors have no conflicts of interest to declare. All co-authors have observed and affirmed the contents of the paper and there is no financial interest to report.

Authors' contribution

Marcelo Muta Hotta: conceptualization, investigation, data curation, visualization, writing – original draft. Marcio de Souza Soares de Almeida: project administration, methodology, supervision, validation, writing – review & editing. José Renato Moreira da Silva de Oliveira: formal analysis, supervision, writing – review & editing. Ricardo Garske Borges: funding acquisition, review.

Data availability

Data sets generated and analyzed during the current study are available from the corresponding author upon reasonable request.

List of symbols and abbreviations

a	Acceleration
g	Gravity
t_0	Initial time
t_f	Final time
v_0	Initial velocity
v_f	Final velocity
v_m	Average velocity
w	Water content
w90_p0.8	Centrifuge test with water content 90% and pressure 80 kPa
w90_p0.9	Centrifuge test with water content 90% and pressure 90 kPa
w100_p0.8	Centrifuge test with water content 100% and pressure 80 kPa
w_p	Water content at plasticity limit
w_l	Water content at liquidity limit
$CaCO_3$	Calcium carbonate
CC	Concentric cylinder
CCT	Concentric cylinder geometry
D_e	Equivalent Diameter
LI	Liquidity index
N	Scale factor
P_1	Checkpoint 1
P_2	Checkpoint 2
R_e	Reynolds number
$R_{eBingham}$	Bingham Reynolds number
SiO_2	Quartz
S	Flow displacement
S_0	Initial flow displacement
Si	Soil sample i
Ti	Rheological test i
USCS	Unified soil classification system
VT	Vane geometry
$\dot{\gamma}$	Shear rate
$\dot{\gamma}_c$	Critical shear rate
μ	Viscosity
μ_1	Viscosity in Regime I of the Bilinear Model
μ_2	Viscosity in Regime II of the Bilinear Model
ρ	Mass density of the fluid
ρ_s	Mass density of the solid
τ	Shear strength of the material
τ_0	Yield stress
τ_c	Critical yield stress
τ_p	Remolded shear strength

References

Acosta, E.A., Tibana, S., de Almeida, M.S.S., & Saboya Junior, F. (2017). Centrifuge modeling ofhydroplaning in submarine slopes. *Ocean Engineering*, 129, 451-458.

Almeida, M.S.S., Oliveira, J.R.M.S., Motta, H.P.G., & Almeida, M.C.F. (2011). Influence of penetration rate

on penetrometer resistance. *Journal of Geotechnical and Geoenvironmental Engineering*, 137, 695-703.

Almeida, M.S.S., Oliveira, J.R.M.S., Rammah, K., & Trejo, P.C. (2013). Investigation of bearing capacity factor of T-bar penetrometer at shallow depths in clayey soils. *Journal of Geo-Engineering Sciences*, 1, 1-12.

Barnes, H.A. (1999). The yield stress – a review or 'παντ ρει' – everything flows? *Journal of Non-Newtonian Fluid Mechanics*, 81, 133-178.

Barnes, H.A., & Nguyen, Q.D. (2001). Rotating vane rheometry: a review. *Journal of Non-Newtonian Fluid Mechanics*, 98, 1-14.

Bjerrum, L. (1972). Embankments on soft ground. In *Proceedings ASCE Conference on Performance of Earth and Earth-Supported Structures* (pp. 1-54). New York: American Society of Civil Engineers.

Bowles, F.A., Faas, R.W., Vogt, P.R., Sawyer, W.B., & Stephens, K. (2003). Sediment properties, flow characteristics, and depositional environment of submarine mudflows, Bear Island Fan. *Marine Geology*, 197, 63-74.

Campos, T.M.P., & Galindo, M.S.V. (2016). Evaluation of the viscosity of tropical soils for debris flow analysis: a new approach. *Geotechnique*, 66(7), 533-545.

Chandler, R.J. (1988). The in-situ measurement of the undrained shear strength of clays using the field vane. In A. F. Richards (Ed.), *Vane shear strength testing in soils: field and laboratory studies* (pp. 150-165). Philadelphia: American Society for Testing and Materials.

De Blasio, F.V., Issler, D., Elverhoi, A., Harbitz, C.B., Ilstad, T., Bryn, P., Lien, R., & Lovholt, F. (2003). Dynamics, velocity and run-out of the giant storegga slide. In *Proceedings Submarine Mass Movements and Their Consequences 1st International Symposium* (pp. 223-230). London: Springer.

Dowdeswell, J.A., Kenyon, N.H., Elverhoi, A., Laberg, J.S., Hollender, F.J., Mienert, J., & Siegert, M.J. (1996). Large-scale sedimentation on the glacier-influenced Polar North Atlantic margins: long-range side-scan sonar evidence. *Geophysical Research Letters*, 23(24), 3535-3538.

Fagundes, D.F., Almeida, M.C.F., Almeida, M.S.S., & Rammah, K.I. (2012). Physical modelling of offshore structures founded on seabed. In *Proceedings ASME 2012 31st International Conference on Ocean, Offshore and Arctic Engineering*. ASME.

Guo, X., Nian, T., Gu, Z., Li, D., Fan, N., & Zheng, D. (2020). Evaluation methodology of laminar-turbulent flow state of fluidized material with special reference to submarine landslide. *Journal of Waterway, Port, Coastal, and Ocean Engineering*, 147(1), 04020048. http://dx.doi.org/10.1061/(ASCE)WW.1943-5460.0000616.

Haldenwang, R., & Slatter, P.T. (2006). Experimental procedure and database for non-Newtonian open channel flow. *Journal of Hydraulic Research*, 44(2), 283-287.

Heezen, B.C., & Ewing, M. (1952). Turbidity currents and submarine slumps, and the 1929 Grand Banks Earthquake. *American Journal of Science*, 250, 849-873.

Heidarzadeh, M., & Satake, K. (2015). New insights into the source of the makran Tsunami of 27 November 1945 from Tsunami waveforms and coastal deformation data. *Pure and Applied Geophysics*, 172, 621-640.

Hotta, M., Almeida, M.S.S., Pelissaro, D.T., Oliveira, J.R.M.S., Tibana, S., & Borges, R.G. (2020). Centrifuge tests for evaluation of submarine-mudflow hydroplaning and turbidity currents. *International Journal of Physical Modelling in Geotechnics*, 20(4), 239-253.

Hsu, S., Kuo, J., Lo, C., Tsai, C., Doo, W., Ku, C., & Sibuet, J. (2008). Turbidity currents, submarine landslides and the 2006 pingtung earthquake off SW Taiwan. *Diqiu Kexue Jikan*, 19(6), 767-772.

Imram, J., Parker, G., Locat, J., & Lee, H. (2001). 1D numerical model of muddy subaqueous and subaerial flow. *Journal of Hydraulic Engineering*, 127(11), 959-968.

Issler, D., De Blasio, F.V., Everhoi, A., Bryn, P., & Lien, R. (2005). Scaling Behaviour of clay-rich submarine debris flow. *Marine and Petroleum Geology*, 22(1-2), 187-194.

Jeong, S.W. (2014). The effect of grain size on the viscosity and yield stress of fine-grained sediments. *Journal of Mountain Science*, 11(1), 31-40.

Jeong, S.W., Leroeil, S., & Locat, J. (2009). Applicability of power law for describing the rheology of soils of different origins and characteristics. *Canadian Geotechnical Journal*, 46, 1011-1023.

Jeong, S.W., Locat, J., Leroueil, S., & Malet, J.P. (2010). Rheological properties of fine-grained sediments: the roles of texture and mineralogy. *Canadian Geotechnical Journal*, 47(10), 1085-1100.

King, E.L., Sejrup, H.P., Haflidason, H., Elverhøi, A., & Aarseth, I. (1996). Quaternary seismic stratigraphy of the North Sea Fan: glacially fed gravity flow aprons, hemipelagic sediments and large submarine landslide. *Marine Geology*, 130, 293-315.

Kobayashi, T., Soga, K., & Dimmock, P. (2015). Numerical analysis of submarine debris flows based on critical state soil mechanics. In *Proceedings of the Frontiers in Offshore Geotechnics III - 3rd International Symposium on Frontiers in Offshore Geotechnics* (pp. 975-980). London: Springer.

Liu, D., Cui, Y., Guo, J., Yu, Z., Chan, D., & Lei, M. (2020). Investigating the effects of clay/sand content on depositional mechanisms of submarine debris flows through physical and numerical modeling. *Landslides*, 17, 1863-1880.

Liujun, Z., Youpiang, Q., Tong, W., & Wei, Z. (2023). Correlation analysis of physical and mechanical parameters of inland fluvial-lacustine soft soil based on different survey techniques. *Applied Rheology (Lappersdorf, Germany)*, 33(1)

Locat, J. (1997). Normalized rheological behaviour of fine muds and their flow properties in a pseudoplastic regime.

In *Proceedings of the 1st International Conference on Debris-Flow Hazards Mitigation* (pp. 260-269). New York: ASCE.

Locat, J., & Lee, H. (2002). Submarine landslides: advances and challenges. *Canadian Geotechnical Journal*, 39, 193-212.

Locat, J., & Lee, H. (2005). Subaqueous debris flow. In M Jakob & O. Hungr (Eds.), *Debris-flow Harzard and Related Phenomena* (pp. 203-245). New York: Springer Praxis Books.

Locat, J., & Lee, H. (2009). Submarine mass movements and their consequences: an overview. In K. Sassa & P. Canuti (Eds.), *Landslides: disaster risk reduction* (pp. 115-142). New York: Springer.

Madlener, K., Frey, B., & Ciezki, H.K. (2009). Generalized reynolds number for non-newtonian fluids. *Progress in Propulsion Physics*, 1, 237-250.

Oliveira, J.R.M., Rammah, K.I., Trejo, P.C., Almeida, M.S., & Almeida, M.C. (2017). Modelling of a pipeline subjected to soil mass movements. *International Journal of Physical Modelling in Geotechnics*, 17(4), 246-256.

Oliveira, J.R.M.S., & Almeida, M.S.S. (2010). Pore-pressure genetation in cyclic T-bar tests on clayey soil. *International Journal of Physical Modelling in Geotechnics*, 10, 19-24.

Rammah, K.I., Borges, R.G., Almeida, M.S.S., Almeida, M.C.F., & Oliveira, J.R.M.S. (2014). Centrifuge modelling of a buried pipeline below an embankment. *International Journal of Physical Modelling in Geotechnics*, 14, 116-127.

Salmanidou, D.M., Georgiopoulou, A., Guillas, S., & Dias, F. (2018). Rheological considerations for the modelling of submarine sliding at Rockall Bank, NE Atlantic Ocean. *Physics of Fluids*, 30(3)

Santoro, A.S., Pellegrino, A.M., Evangelista, A., & Coussot, P. (2012). Rheological behavior of reconstituted pyroclastic debris flow. *Geotechnique*, 62(1), 19-27.

Satake, K. (2012). Tsunamis generated by submarine landslides. In *Proceedings Submarine Mass Movements and Their Consequences 5th International Symposium* (pp. 475-484). London: Springer.

Sigh, A., & Mitchell, J.K. (1968). General stress-strain-time function for soils. *Journal of the Soil Mechanics and Foundations Division*, 94(1), 21-46.

Sørlie, E.R., Hartnik, L.O., Tran, Q., & Eiksund, G.R. (2022). Rheological parameters for submarine landslide materials. In *Proceedings 10th International Conference on Physical Modeling in Geotechnics.* Boca Raton: CRC Press.

Steffe, J.F. (1996). *Rheological methods in food process engineering* (2nd ed.). East Lansing: Freeman Press.

Tailling, P.J., Masson, D.G., Sumner, E.J., & Malgesini, G. (2012). Subaqueous sediment density flows: depositional processes and deposit types. *Sedimentology*, 59(7), 1937-2003.

Takahashi, T. (2007). *Debris flow: mechanics, prediction and countermeasures.* London: Taylor & Francis/Balkema.

Tsugawa, J.K., Romano, R.C.O., Pileggi, R.G., & Boscov, M.E.G. (2019). Review: rheology Concepts applied to geotechnical engineering. *Applied Rheology*, 29(1), 202-221.

Vorren, T.O., Hald, M., & Lebesbye, E. (1988). Late Cenozoic enviroments in the Barent Sea. *Paleoceanography*, 3(5), 601-612.

Widjaja, B., & Lee, S.H.H. (2013). Flow box teste for viscosity of soil in plastic and viscous liquid state. *Soil and Foundation*, 53(1), 35-46.

Yang, H.J., Wei, F.Q., & Hu, K.H. (2015). Comparison of rheometric devices for measuring the rheological parameters of debris flow slurry. *Journal of Mountain Science*, 12(5), 1125-1134.

Zakeri, A., Si, G., Marr, J.D.G., & Hoeg, K. (2010). Experimental investigation of subaqueous clay-rich debris flows, turbity generation and sediment deposition. In *Proceedings Submarine Mass Movements and Their Consequences 4th International Symposium* (pp. 105-116). London: Springer.